Available online at www.sciencedirect.com
ScienceDirect
Geochimica et Cosmochimica Acta 75 (2011) 1942–1956
Geochimica et Cosmochimica Acta
www.elsevier.com/locate/gca

Distribution and speciation of gold in biogenic and abiogenic calcium carbonates – Implications for the formation of gold anomalous calcrete

Frank Reith [a,b,*], Barbara Etschmann [a], Robert C. Dart [a], Dale L. Brewe [c], Stefan Vogt [c], Andreas Schmidt Mumm [a], Joël Brugger [a,d]

[a] Centre for Tectonics, Resources and Mineral Exploration (TRaX), School of Earth and Environmental Sciences, The University of Adelaide, North Terrace, SA 5005, Australia
[b] CSIRO Land and Water, Environmental Biogeochemistry, PMB2, Glen Osmond, SA 5064, Australia
[c] APS, Argonne National Laboratory, Argonne, IL 60439, USA
[d] South Australian Museum, North Terrace, Adelaide, SA 5000, Australia

Received 12 April 2010; accepted in revised form 10 January 2011; available online 18 January 2011

Abstract

Calcrete (pedogenic Ca carbonate) is an important sampling medium for geochemical gold (Au) exploration in semi-arid and arid regions of Australia, because it is widespread, easy to sample and calcium (Ca) shows a strong positive correlation with Au, but not with base metals, in calcrete overlying buried Au mineralization. In this study we show that the formation of Au-anomalous calcrete can be biomediated through the activity of resident microorganisms, and may not simply be the result of passive nucleation on inactive cells or evapotransporative processes. Calcified microfossils are highly abundant in calcrete from the Barns Au-prospect in South Australia. These microfossils are morphological analogues of calcified cells and biofilms formed in laboratory experiments conducted with active bacterial cultures enriched from Au-anomalous calcareous sand from the Barns prospect. Calcium carbonates precipitated by these cultures consisted mostly of calcite, which is the main carbonate mineral in calcrete. Synchrotron micro-X-ray fluorescence (S-μXRF) mapping was used to assess the distribution of Au, Zn, Ca and other metals in Ca carbonates precipitated by active bacterial cultures. On a μm-scale the distribution of Au was heterogeneous in these Ca carbonates and differed from base metal distribution, thus mimicking the spatial separation of these metals observed in calcrete. The speciation of Au in Ca carbonates precipitated by active bacteria was measured using micro-X-ray absorption near edge structure spectroscopy (μ-XANES) and resembled that observed in Au-anomalous calcrete closely. While metallic Au was observed in Au 'hotpots', ionic Au was detected in the halo surrounding the 'hotspot'. In contrast, the precipitates produced in the presence of dead bacterial cells or by raising solution pH or pCO_2, i.e., hydroxylapatite, portlandite and vaterite, respectively, did not reflect the mineralogy of calcrete. Gold distribution and speciation in vaterite, formed by raising pCO_2, were homogenous and did not reproduce the variation observed in calcrete and Ca carbonates precipitated by active cells. Increasing the supersaturation with respect to Ca in solution by incremental drying of the medium produced only X-ray amorphous precipitates, or hydroxylapatite in the presence heat-killed cells. In conclusion, this study shows that active microbial processes that combine biogenic Ca carbonatogenesis with Au precipitation are likely to drive the formation of Au-anomalous calcrete.

1. INTRODUCTION

Secondary pedogenic carbonate (calcrete) occurs in many regions of southern Australia that are located below 30°S

* Corresponding author at: CSIRO Land and Water, Environmental Biogeochemistry, PMB2, Glen Osmond, SA 5064, Australia. Tel.: +61 8 8303 8469; fax: +61 8 8303 8550.
E-mail address: Frank.Reith@csiro.au (F. Reith).

0016-7037/$ - see front matter
doi:10.1016/j.gca.2011.01.014

latitude in semi-arid and arid areas, i.e., areas with less than 500 mm rainfall per annum (McQueen et al., 1999). The term "calcrete" used in this manuscript is an encompassing term for secondary, pedogenic carbonate in the terrestrial environment, and is equivalent to the regolith carbonate described by Butt and Smith (1992). Calcrete occurs in a variety of forms, such as calcareous sands in aeolian transported cover materials, carbonate powders and rhizoliths, nodular concretions, mottled horizons and discrete hardpans (McQueen et al., 1999). It has become an important sampling medium for geochemical exploration for Au in Australia, because it is widespread, easy to sample and bulk geochemical analyses show a strong positive correlation between Ca and Au in calcrete overlying buried Au mineralization (Lintern and Butt, 1993). A number of economically important deposits have been discovered as a consequence of calcrete sampling, e.g., the Challenger deposit and the Tunkillia, Baggy Green and Barns prospects in South Australia. Concentrations of Au in calcrete typically lie between 0.5 and 500 μg kg^{-1}. At these concentrations Au is finely dispersed throughout carbonate crystallites and displays a reduced nugget effect (Schmidt Mumm and Reith, 2007). Other trace metals, e.g., Ag, As, Cu, Ni or U, show no systematic association with secondary regolith Ca carbonates (Schmidt Mumm and Reith, 2007). This suggests a specific pathway of Au precipitation with Ca during the formation of calcrete as well as a decoupling from other metals during this process.

Biomineralization of secondary Ca carbonates (Ca carbonatogenesis) is commonly mediated by microorganisms, such as bacteria, fungi, actinomycetes and algae (e.g., Zhou and Chafetz, 2009). Bacterial carbonatogenesis has been reported from many environments, such as agricultural and forest soils, marine and fluvial sediments as well as saline soils and lakes (Boquet et al., 1973; Krumbein, 1979; Morita, 1980; Rivadeneyra et al., 1993; Castanier et al., 1999, 2000; Martín-Algarra and Sánchez-Navas, 2000; Zhou and Chafetz, 2009). Bacteria also play an important role by providing nucleation sites for the formation of Ca carbonates (Braissant et al., 2003; Hammes et al., 2003; Reith et al., 2009b). The importance of microbial calcification for the formation of calcrete in South Australia was first demonstrated using scanning electron microscopy (SEM), which showed that calcified microbial fossils forming dense mats of micritic calcrete occurred at numerous sites (Phillips et al., 1987). Similar biogenic morphologies were ubiquitous and highly abundant in calcrete from subhumid to arid regions in Texas, USA (Zhou and Chafetz, 2009).

Schmidt Mumm and Reith (2007) and Reith et al. (2009b) developed an inclusive biogeochemical/geomicrobial model for Au anomalous calcrete formation. At the heart of this model are microbial processes, i.e., heterotrophic and autotrophic metabolic pathways combined with active and/or passive biomineralization, which lead to the formation of Ca carbonates (Reith et al., 2009b). One of the most widespread and best understood mechanisms is Ca carbonatogenesis via urea decomposition (ureolysis), which appears to be directly linked to Au mobilization and re-precipitation (Schmidt Mumm and Reith, 2007). The formation of amino acids, which are known to mobilize Au, is a result of the decomposition of plant-derived organic matter (Reith and McPhail, 2006). The microbially-mediated ammonification of these amino acids, and the formation and decomposition of urea leads to the destabilization of these Au-complexes and the co-precipitation of Au with Ca^{2+} and CO_3^{2-} on the associated cells acting as nucleation sites (Schmidt Mumm and Reith, 2007). In this process, Au is sorbed by bacterial cells and carbonates leading to the physical entrapment inside the growing Ca carbonate crystals (Reith et al., 2009b). Gold-(I/III)-halide complexes are considered to be major contributors to the observed Au mobility in arid and semi-arid surface environments overlying mineralization (Usher et al., 2009). Bacteria are known to rapidly adsorb these Au(I/III)-complexes, and some metallophilic bacteria have been shown to actively catalyze their reductive precipitation (Lengke et al., 2006; Reith et al., 2009a).

Despite the known importance of microorganisms for Ca carbonatogenesis, the model for the formation of Au-anomalous calcrete proposed in a number of studies ascribes the formation of calcrete, as well as the distribution of Au therein, solely to the influence of evapotranspirative processes (Achyuthan, 2003; Lintern et al., 2006, 2009; Moussavi-Harami et al., 2009). In this model the observed decoupling of Au from base metals is attributed to an abiogenic pH effect (Lintern, 2001): with increasing pH the mobility of base metals decreases, while Au mobility increases, although Lintern (2001) does not provide a mechanistic explanation for these differences. Strong support for the evapotranspiration model was drawn from observations of Au distribution and speciation in a calcareous profile at the Bounty Gold Deposit in Western (Lintern et al., 2009). Bulk samples (kg) confirmed a strong positive correlation between Au and Ca (Lintern et al., 2009). However, synchrotron μ-XRF mapping of Ca, Au and other metals combined with Au L-edge μXANES spectroscopy did not confirm this observation at the sub-mm scale, revealing instead the presence of μm-sized metallic Au as well as ionic Au concentrated in high-porosity areas such as root tunnels (Lintern et al., 2009). This spatial separation of Au and Ca at μm-scale led Lintern et al. (2009) to conclude that Au and Ca are behaving similarly but independently. This small-scale inhomogeneity in natural calcrete appears to contrast with analyses of the Au distribution in experimentally grown biogenic Ca-carbonates, that showed that Au was homogenously distributed at spatial resolutions possible with LA–ICP–MS (>30 μm^2; Reith et al., 2009b). This led Lintern et al. (2009) to conclude that the spatial separation between Au and Ca at μm-scale implies that Au-anomalous Ca carbonates form via abiogenic, evapotranspirative processes. Hence, the aim of this study is to investigate the consequences of the observed μm-scale distribution and speciation of Au in calcrete for Reith et al., 2009b's biogeochemical/geomicrobial model by: (i) comparing the distribution and speciation of Au in Ca carbonates precipitated by active bacterial cultures to that in Ca carbonates formed abiogenically, in the presence of dead cells and in calcrete; as well as (ii) comparing morphologies and mineralogical compositions of experimental precipitates with those of calcrete.

2. MATERIALS AND METHODS

2.1. Description of field sites

2.1.1. The Barns Au in calcrete anomaly

The Barns Au prospect is located on northern Eyre Peninsula, at S 32° 55′ 40″ and E 135° 24′ 45″, approximately 340 km NW of Adelaide in South Australia. The climate in the area is semi-arid with summer temperatures of 30–32 °C and winter temperatures of 17–18.5 °C, and average annual rainfall lies around 300 mm (Australian Government, Bureau of Meteorology, 2005). A detailed description of the exploration history, geology, mineralogy, regolith and calcrete is given in Drown (2003) and Schmidt Mumm and Reith (2007), so a summary is provided here. The Barns Au anomaly was established through calcrete sampling by Adelaide Resources Ltd. The area of the prospect is characterized by low relief of plains or swales interrupted by linear dunes consisting of clay-rich aeolian sands and silts that can be up to several kilometers long and up to 10 m high (Twidale and Wopfner, 1990). In the study area the uppermost regolith units contain calcrete, which occurs as: (i) incrustation of the soil and saprock; (ii) nodular Ca carbonate rich concretions within the transported material; and (iii) Ca carbonate rich sands within the transported overburden. Specimens for microscopic analyses were obtained in January 2010 using field-sterile sampling techniques (Reith et al., 2009b). Calcium carbonates are present as incrustation on detrital quartz grains, and carbonate content of the sands increases with depth. Anomalously high Au concentrations (2.5–50 $\mu g\ kg^{-1}$) in calcareous sands overlying Au mineralization showed a correlation of Au with Ca, which was linked to the authigenic formation of Ca carbonates that occur as micritic calcite (Schmidt Mumm and Reith, 2007). The pH measured in watery extracts (1:5 w:v) increase with depth from pH 7.5–10. Soil conductivity also increased with depth and extractable solutions were moderate to highly saline and highly alkaline. The dunes on the prospect that are not used for farming are covered by native vegetation consisting of mallee eucalypts, e.g., *Eucalyptus incrassata* and *Melaleuca uncinata*, and *Spinifex* spp. Underlying the dunes at the Barns prospect is weathered bedrock of the Tunkillia Suite. The weathering depth is up to 50 m (Drown, 2003). The intrusive rocks of the Tunkillia (1690–1680 Ma) and the Hiltaba Suite granites (~1590 Ma) form a small number of prominent outcrops in the area. The Tunkillia Suite gneisses or granodioritic rocks host a primary hydrothermal Au mineralization in quartz-pyrite veins.

2.1.2. The White Dam Au in calcrete anomaly

The White Dam Au in calcrete anomaly is in the southern margin of the Curnamona Province, at S 32° 05′ 35″ and E 140° 34′ 31″ (approximately 350 km NNE of Adelaide in South Australia). The climate in the area is semi-arid with temperatures and annual rainfall similar to the Barns site (Australian Government, Bureau of Meteorology, 2010). A detailed description of the exploration history, geology, mineralogy, regolith and calcrete is given in Dart (2009), so a summary is provided here. The White Dam anomaly is in an area of low relief with minor bedrock exposure. Alluvial sheet-flow sediments, around two meters thick, are the dominant regolith materials. Calcrete occurs in the uppermost regolith units as incrustations and accumulations of small bi-refringent crystals or crystallitic fabric that fills many of the voids. In the highly calcareous horizons, with Ca carbonate contents of up to 20 wt.%, calcrete commonly occur as nodules that are 15–30 mm in diameter. Calcrete samples were collected from the calcareous Bk horizons within the mineralized zone. The sampled profile was approximately three meters deep and consisted of a thin A1 horizon, a sandy clay B1 horizon that becomes calcareous with depth and changes gradually to a B2 horizon followed by a highly calcareous Bk horizon with Ca carbonate content of up to 18.6 wt.%. The pH measured in watery extracts (1:5 w:v) increased with depth from pH 8.8 to 10.3. Soil conductivity increased with depth and extractable solutions were moderately to highly saline and highly alkaline. In bulk analyses of Au concentrations within carbonate mottles several hundreds of $\mu g\ kg^{-1}$ were detected (Hill et al., 1998). Vegetation in the area is dominated by a chenopod shrubland consisting of bladder saltbush (*Atriplex vesicaria*), black bluebush (*Maireana pyramidata*) and pearl bluebush (*Maireana sedifolia*). The geology of the area consists of meta-sedimentary rocks of the Palaeoproterozoic Willyama Supergroup, which hosts the primary Au mineralization (Flint and Parker, 1993). Primary Au mineralization is located in a stockwork of pyrite and chalcopyrite veins that have been oxidized to 50 m below the surface (Cooke, 2003).

2.2. Ca carbonate precipitation experiments

Calcium carbonate precipitation experiments (Experiments 1–10) were conducted in triplicate using 50 mL urea medium in 100 mL Erlenmeyer flasks following the procedures described in Reith et al. (2009b). The urea growth medium, contained [$g\ L^{-1}$]: nutrient broth (Difco), 3; urea, 20; NH_4Cl, 10; $NaHCO_3$, 2.12, and pH was adjusted to 8 after autoclaving. In all experiments flasks were incubated on a shaker at 30 °C and 100 revolutions per minute (rpm) in the dark and samples were collected after 120 h. In Experiment 1, i.e., Ca carbonate precipitation with active cells, the medium was amended with 4.4 g of $CaCl_2\ kg^{-1}$ of medium. In Experiment 2, i.e., Ca carbonate and Au precipitation with active cells, 250 μg Au(III)-$chloride_{(aq)}\ kg^{-1}$ was added in addition to $CaCl_2$. The media were then inoculated with 50 μL of a bacterial enrichment culture obtained from calcareous sand at 0.64 m depth at the Barns Au prospect. The culture consisted predominantly of *Bacillus pichinotyi* and *Bacillus lentus*, which made up more than 75% of clones in a clone library (Reith et al., 2009b). The composition of the enrichment culture closely reflected the composition of the natural communities resident in the sampling profile, which consist uniformly of alkaliphylic, halotolerant *Bacillus* spp. (Reith et al., 2009b). Calcium carbonates from a previous study (Reith et al., 2009b) precipitated using the same enrichment culture under similar conditions but amended with a Au-aspartic acid complex were also studied (Experiment 3). To individually assess the influence of abiogenic factors

on Au-anomalous Ca carbonate formation, experiments without active cells were amended with 4.4 g $CaCl_2$ and 250 μg Au(III)-chloride$_{(aq)}$ kg^{-1} of medium and conducted in urea medium under otherwise similar conditions. Experiment 4 was a sterile control experiment similar to Experiment 2 but without cells. Precipitation of minerals on inactive cells has also been proposed to lead to the formation of Ca carbonates, especially under highly evaporative conditions (Zavarin, 2000). This was tested in Experiments 5 and 6. For these experiments the bacterial cultures were first grown in urea medium without $CaCl_2$ or Au(III)-complexes. Cells were then harvested by centrifugation and heat-killed by wet-autoclaving for 1 h at 125 °C. Dead cells were then re-suspended in urea medium amended with $CaCl_2$ and Au(III)-chloride$_{aq}$ and incubated for 120 h (Experiment 5). To assess the influence of dead cells combined with evaporation, flasks containing dead cells and $CaCl_2$ and Au(III)-complexes were subjected to drying at 50 °C (Experiment 6). Increasing evaporation as well as changes to pCO_2 and pH have been proposed as abiotic pathways of Ca carbonate formation (Langmuir, 1997; Königsberger et al., 1999). To test the influence of evaporation followed by extreme supersaturation of Ca, replicate flasks were subjected to evaporation in a drying oven at 50 °C (Experiment 7). To test the influence of increasing pH on Ca carbonate precipitation, the pH in the medium was raised stepwise in replicate flasks to pH 10.0, 11.00 and 12.00 using sterile 10 M NaOH solution (Experiment 8). To assess the influence of increasing pCO_2 media were amended with 250 μg Au(III)-chloride$_{(aq)}$ kg^{-1} and 4.4 g $NaCO_{3aq}$ kg^{-1} of medium (Experiment 9); Experiment 10 was amended with 2500 μg Au(III)-chloride$_{(aq)}$ kg^{-1} and 4.4 g $NaCO_{3aq}$ kg^{-1} of medium.

2.3. Analyses of precipitates

Cell suspension was harvested from Experiments 1 and 2 and stored in fixative consisting of 1.25 wt.% glutaraldehyde, 4 wt.% paraformaldehyde and 4 wt.% sucrose in 1 × PBS buffer. 0.5 mL of fixed calcified cells and biofilms were filtered through 0.2 μM nucleopore filter. Filters were prepared for SEM analysis using critical point (CDP) drying after a series of 70, 90 and two times 100% ethanol dehydration steps using a BALTEC CPD 300 (Adelaide Microscopy, University of Adelaide, Australia). Filters were mounted on adhesive carbon tape attached to sample holders and Pt coated (3 nm).

Mineral precipitates from all experiments were harvested by centrifugation at 4500 rpm for 10 min. Calcium carbonates harvested by centrifugation were washed three times with double deionized water and air-dried in a dust-free environment. These samples were used for a range of analyses including SEM, X-ray diffraction (XRD), Laser Ablation Inductively Coupled Plasma Mass Spectrometry (LA–ICP–MS), S-μXRF and μXANES as described below. Samples for SEM and SEM with X-ray microanalysis (SEM–EDS) were mounted on adhesive C, and coated with Pt, Ir or remained uncoated. No additional preparation was performed before secondary electron imaging using a Philips XL30 SEM (Philips, Netherlands) and focused-ion-beam (FIB)–SEM (Helios NanoLab DualBeam, FEI, Netherlands) at accelerating voltages of 5–15 kV. X-ray microanalysis analyses were performed at working distances of 20 and 4 mm with the XL30 and Helios SEMs at 20 kV; the results confirmed the presence of Ca and C in these samples. The morphology of calcified cells and carbonates/calcrete samples was classified according to the system described in Wright (1997) and Zhou and Chafetz (2009).

X-ray diffraction data were collected using a laboratory Huber Imaging Plate Guinier Camera G670 with Co Kα1 radiation. The XRD patterns were recorded for 1 h with $10° \leqslant 2\theta \leqslant 100°$ at 0.005° resolution. The data were analyzed using the XPLOT (v 1.27) software.

Mineral precipitates produced in the laboratory and natural calcrete samples were mounted in epoxy resin and polished whole mounts were prepared for imaging and Au analyses using LA–ICP–MS. LA–ICP–MS was conducted at Adelaide Microscopy (University of Adelaide) using a high performance New Wave Nd Yag 213 UV laser coupled with an Agilent 7500cs ICP–MS equipped with a He collision cell for removal of matrix interferences. Material was ablated from individual Ca carbonates crystals as well as calcrete samples. Calcium and Au concentrations were quantified using the NIST standard glasses 612a and 612b (National Institute of Standards and Technology, USA). Based on the LA–ICP–MS results 100 μm thick polished sections were prepared from whole mounts for S-μXRF and μ-XANES.

Synchrotron X-ray fluorescence (S-XRF) data were collected at the undulator 2-ID-E and 20-ID-B microprobes at the Advanced Photon Source (APS) in Chicago. The APS is a 7 GeV ring that operates in top-up mode with an approximately constant current of 102 mA. The 2-ID-E microprobe was set-up with a Si(220) monochromator and tuned to an incident beam energy of 12.0 keV. This energy was chosen as it is above the Au L_3 edge. 2-ID-E is a branch beam-line that uses a silicon crystal beam splitter as a single bounce monochromator. X-rays were focused with a Fresnel zone plate with a focal length of 10 cm at 12.0 keV, resulting in a focused beam spot of $\sim 0.32 \times 0.26$ μm^2. A step size of 1 μm in x and y direction was used. An order-sorting aperture intercepted higher diffraction orders and, in conjunction with a central stop, blocked the unfocussed beam. A single element Ge energy-dispersive detector was located at ~90° to minimize detection of the scattered beam. It was fitted with a conical collimator large enough to accept scattered X-rays. A NIST 1832 standard foil (National Bureau of Standards NBS/NIST, Gaithersburg, MD) was used to calibrate the energies and constrain the detector solid-angle and absorption due to the air path.

The 20-ID-B microprobe was set-up with a Si monochromator and tuned to an incident beam energy of 14.5 keV. Kirkpatrick–Baez mirrors were used to focus the beam to a size of 3.5×3 μm^2. A step size of 1.5 μm in x and y direction was used for minerals precipitated in the laboratory experiments; for calcrete samples a step size of 1.0 μm in x and y direction was used. The calculated absorption length was 152 μm, hence the resulting maps provide a two-dimensional representation of element distribution throughout the entire depth of the 100 μm thin section. A seven-element Ge array solid-state detector was

located at ~90° to detect fluorescent photons. The BHVO-2G micro-analytical reference material from the United States Geological Survey was used to calibrate the energies and constrain the detector solid-angle and absorption due to the air path. Imaging was conducted by raster scanning the sample through the focused beam, and full spectra (as opposed to simply acquiring regions-of-interest (ROI)) were acquired at each scan position at both microprobes. Micro-XRF imaging data were projected onto elemental images using the dynamic analysis (DA) method (Ryan and Jamieson, 1993; Ryan, 2000) in the GeoPIXE software package, which uses a standardless analysis approach (Ryan et al., 2005). The DA technique uses a matrix-transform-algorithm that deconvolutes overlapping elemental lines and subtracts background, tailing and escape peaks, and other detector artefacts to reconstruct individual elemental images. By using multiple lines per element, this method benefits from better counting statistics and it is possible to distinguish between elements that have some overlapping X-ray lines which are traditionally difficult to separate using ROIs. Pearson correlation coefficients for elements were calculated in Microsoft Excel after exporting results for each analysis from GeoPIXE.

Gold L3-edge (11919 eV) μXANES data were measured at 20-ID-B. Data were measured in fluorescence mode with a seven-element Ge array solid-state detector and the incident beam intensity I_0 was measured with an ionization chamber. Data were collected from 11720 to 11901 in 10 eV steps to measure the background and then from 11901 to 12000 eV, using 0.3 eV steps; counting for 4 s at every point. At 20-ID-B a beam splitter is used to siphon off a small fraction of the incoming beam. This enables a calibration foil (Au in this instance) to be measured in conjunction with each data set making it possible to determine any shift in the energy. Background subtraction, normalization of XANES spectra and linear combination analysis (LCF) were conducted in ATHENA, which is a part of the Ifeffit package (Ravel and Newville, 2005). The XANES spectra were compared with Au standards that had been measured previously (Reith et al., 2009a) – the energy offsets between the spectra from different experiments were accounted for by setting the first maximum in the derivative of the XANES spectrum of the measured the Au foils at all beamlines to be at 11919 eV.

3. RESULTS

3.1. Micro-morphology and mineralogy of mineral precipitates formed in the laboratory and of calcrete

Calcareous crusts as well as nodular and hardpan calcrete from the Barns Au-in-calcrete are composed of micritic calcite. In these calcrete samples, needle- and spherulite-like structures, fossilized rhizoids and remnants of microbial communities (microfossils) consisting of calcified filamentous fungal and rod-shaped bacterial structures are abundant and well-preserved (Fig. 1A–C). Calcified bacterial rods are between 0.4 and 1.8 μm in length and form extensive mats of calcified biofilms (Fig. 1C) as well as spherical conglomerates (Fig. 1D). Microcrystalline calcite that encrust rhizomorphs and filaments that radiate from the central hollow area occur in a variety of crystal habits, such as anhedral and rhombohedral crystals as well as euhedral blades and needles (Fig. 1A and B).

Calcium carbonates precipitated in the laboratory by active bacterial cultures displayed similar morphologies (Fig. 1E and F). Rod-shaped calcified cells were between 1 and 3 μm in length (Fig. 1E) and acted as nuclei for the formation of Ca carbonate crystals. Increased deposition of Ca carbonates by conglomerates of cells led to the formation of spherical Ca carbonates, which closely resembled the morphologies observed in the calcrete samples (Fig. 1E and F). Growth of new generations of Ca carbonate precipitating cells led to the formation of calcified microbial mats (Fig. 1F).

The mineralogy of Ca containing precipitates varied strongly between the different experiments. Calcite was the only mineral precipitated by active bacterial cultures in urea medium amended with $CaCl_2$ and Au-complexes (Experiments 2 and 3; Table 1, Figs. 2A and 3A). In Experiment 1, with active cells but no Au, approximately 75 wt.% calcite and 25 wt.% vaterite spherules were precipitated (Table 1). Vaterite spherules were between 5 and 20 μm in diameter and resembled spherules formed in Experiments 9 and 10. In Experiments 9 and 10 pCO_2 was raised in the absence of cells and vaterite spherules were the dominant minerals formed (Table 1; Fig. 4A and B). No precipitates were formed in a sterile medium without cells (Experiment 4). When the cell-free medium was evaporated (Experiment 7) no crystalline precipitates were observed, despite supersaturated conditions with respect to all $CaCO_3$ polymorphs, i.e., calcite, vaterite and aragonite (Table 1 and Stumm and Morgan, 1996). Evaporation in the presence of dead cells (Experiment 6) yielded finely grained hydroxylapatite (<1 μm) as the only crystalline precipitates; in addition X-ray amorphous precipitates were observed. In Experiment 5 conducted in the presence of dead cells without evaporation, hydroxylapatite was also the only crystalline precipitate formed (Table 1). Increasing the pH in Experiment 8 led to the formation of a precipitate at pH 12. The precipitate consisted mostly of fine-grained (0.1–5 μm-sized), hexagonal platy portlandite crystals (Table 1).

3.2. Distribution and speciation of Au in Ca carbonates formed by active bacterial cultures

Biogenic Ca carbonates were harvested after 120 h of incubation to assess the distribution and speciation of Au. Individual crystals formed in Experiments 2 ranged from 100 to 200 μm in diameter (Figs. 2A and 3A). Calcium carbonate crystals from Experiment 2 were enriched by a factor of up to 400 with respect to Au compared to its concentration in the medium (Table 1; 250 μg kg^{-1}). Gold concentrations varied between individual crystals and ranged from 15.2 to 110.9 mg kg^{-1} in Experiment 2 and between 1.6 and 194.2 mg kg^{-1} in Experiment 3 (Table 1). No significant differences were observed between different spots on the same crystallite or in the LA–ICP–MS profiles, with counting rates remaining flat with respect to Au. This confirmed the results of an earlier study by Reith et al.

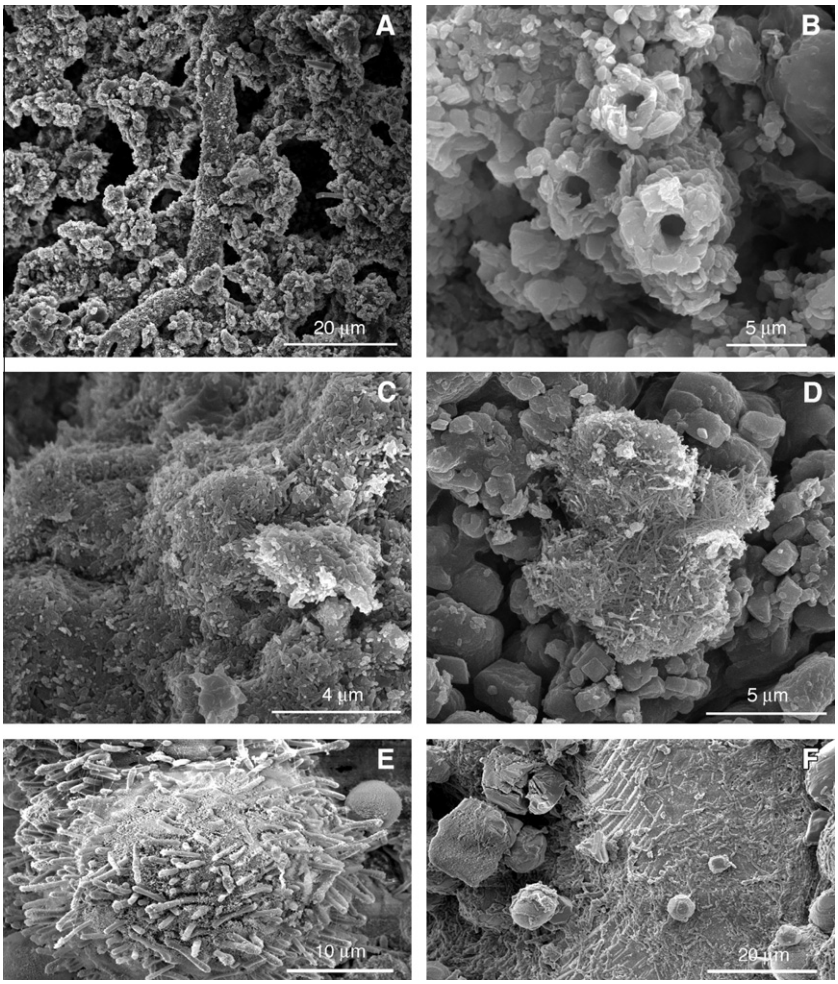

Fig. 1. Secondary electron micrographs of biogenic Ca carbonates from the Barns Au deposit in South Australia (A–D) and of bacterial cells, calcified biofilms, and biogenic Ca carbonates precipitated by active bacterial cultures in Experiment 2 (E and F). (A) Layer of tubiform calcified filaments forming on rounded quartz sand grain forming the matrix of the micritic calcite. (B) Tubiform calcified filaments exhibiting a smooth inner wall with thick encrustations of rhombohedral calcite crystals in a radiating pattern. (C) Microbial mat composed of calcified micro-rods varying between 0.5 and 1.8 µm in length. (D) Calcified micro-rods (0.5–2.0 µm in length) forming spherical nodules. (E) Progressive calcification of rod-shaped bacterial cells forming spherical Ca carbonate nodules. (F) Calcified biofilms consisting of layers of calcified cells.

(2009b), which had shown that Au was uniformly distributed within individual crystals at the resolution of the LA–ICP–MS (>30 µm^2).

In subsequent analyses S-µXRF was used to map the distribution and concentration of Ca, Au, Zn and base metals on a µm-scale (e.g., Fe, Mn, Ni, Cu, Zn; Figs. 2B–E and 3C–F). A round Ca carbonate from Experiment 2 (approximately 100 µm in diameter) was chosen for ultra-high resolution mapping at beamline 2-IDE (APS, Chicago, USA, Fig. 3A), because it was typical for Ca carbonates precipitated in Experiment 2, and a morphological analogue the biogenic Ca carbonates forming the Barns calcrete (Fig. 1B and C). While Au was generally finely dispersed throughout the mapped area, demonstrating a reduced nugget effect, accumulations ('hot-spots') of Au were observed in distinct areas (Fig. 2B and E). Zinc was chosen as a model for base metal distribution in the overlay images, because Zn was quantifiable in all samples (Figs. 2D, 3E, 4F, 5C and 6E). Other trace metals, e.g., Cr, Ni, Cu and Mn, were quantifiable in some experiments and showed a positive correlation with Zn (data available on request). Synchrotron µ-XRF maps (Figs. 2B–E and 3C–F) showed that in Ca carbonates precipitated by active bacterial cultures of Au and Zn were not associated, which was expressed by low correlation coefficients for Au and Zn that lie between 0.1 and 0.2. The elemental images revealed that the Au and Ca maxima did not coincide, but occurred in close spatial proximity to each other (Figs. 2B and 3B); however, Ca and Au showed no or only a weak correlation with correlation coefficients 0.1 and 0.4 for data shown in Figs. 2B and 3B. No correlation between Ca and Zn data and Au and Zn was observed (correlation coefficients between 0.1 and 0.2). Samples from Experiment 3 (amended with Au-aspartic acid complexes) also displayed a differentiated Au distribution (Fig. 5A and D), and a weak positive correlation between Au and Ca (correlation coefficient of 0.4; Fig. 5).

Table 1
Differences in incubation conditions of Experiments 1–10, mineralogy of Ca containing precipitates and concentration of Au (average ± standard deviation and range) in precipitates based on the analyses of nine crystals using LA–ICP–MS.

Experiment	Differences in experimental conditions	Calcite (%)	Vaterite (%)	Portlandite (%)	Hydroxylapatite (%)	Gold (mg kg^{-1})
1	Live cells, no Au	75.0 ± 1.0	24.9 ± 0.7	n.d.[a]	n.d.	n.d.
2	Live cells, 250 μg Au(III)-chloride$_{(aq)}$ kg^{-1} medium	99.6 ± 1.0	n.d.	n.d.	n.d.	42.3 ± 31.4 (15.2–110.9)
3	Live cells, 100 μg Au(III)-aspartic acid kg^{-1} medium	99.2 ± 0.8	1.8 ± 0.4	n.d.	n.d.	59.4 ± 49.7 (1.6–194.2)
4	No cells, 250 μg Au(III)-chloride$_{(aq)}$ kg^{-1} medium	n.d.	n.d.	n.d.	n.d.	n.d.
5	Dead cells, 250 μg Au(III)-chloride$_{(aq)}$ kg^{-1} medium	n.d.	n.d.	n.d.	100.0 ± 1.0	n.a.[b]
6	Dead cells, 250 μg Au(III)-chloride$_{(aq)}$ kg^{-1} medium, evaporation	n.d.	n.d.	n.d.	100.0 ± 1.0	n.a.
7	No cells, 250 μg Au(III)-chloride$_{(aq)}$ kg^{-1} medium, evaporation	n.d.	n.d.	n.d.	n.d.	n.d.
8	No cells, 250 μg Au(III)-chloride$_{(aq)}$ kg^{-1} medium, pHs 10–12	26.0 ± 1.0	3.7 ± 0.6	70.0 ± 1.0	n.d.	32.0 ± 10.4 (17.1–46.9)
9	No cells, 250 μg Au(III)-chloride$_{(aq)}$ and 4.4 g $NaCO_3$ kg^{-1} medium	18.8 ± 0.2	81.2 ± 0.5	n.d.	n.d.	1.6 ± 0.7 (0.5–2.9)
10	No cells, 2500 μg Au(III)-chloride$_{(aq)}$ and 4.4 g $NaCO_3$ kg^{-1} medium	18.4 ± 0.2	81.6 ± 0.5	n.d.	n.d.	74.3 ± 2.6 (69.3–77.1)

[a] n.d., not detected.
[b] n.a., not analyzed.

Correlation coefficients for Ca and Zn and Zn and Au were 0.1.

XANES spectroscopy was conducted to assess the speciation of Au in samples from Experiment 2 (Fig. 3C). The spectra were compared to standard spectra obtained for metallic Au and seven Au(I/III)-compounds (Fig. 3C). Differences in Au speciation occurred depending on the location of the Au in the sample (Fig. 3C). Spectra obtained from the centre of a Au 'hotspot' showed metallic characteristics, whereas spectra displaying ionic Au characteristics were detected in the halo surrounding the Au 'hotspot' (Fig. 3F). This was confirmed by LCF, which showed that the proportion of ionic Au increased with distance from the metallic Au hotspot (Table 2).

3.3. Distribution and speciation of Au in Ca carbonates formed in the absence of active cells and in calcrete from White Dam

Only raising pCO_2, in the absence of active bacterial cells (Experiments 9 and 10) led to the precipitation of Ca carbonates (Fig. 4A and B). In both experiments approximately 80 wt.% spherical vaterite and 20 wt.% calcite were precipitated (Table 1). None of the other experiments conducted in the absence of active bacterial cells yielded predominantly Ca carbonates. Experiments 9 and 10 showed enrichment factors of 5 of 25, respectively, between to Au concentration in Ca carbonates and the medium (Table 1), and LA–ICP–MS analyses showed that Au was uniformly distributed in the samples. This homogeneity was confirmed at μm-scale by S-μXRF mapping, which also showed high spatial correlation (correlation coefficient of 0.8) between the Au and Ca (Fig. 4D–G). Correlation coefficients for Au and Zn, and Ca and Zn were −0.1 and −0.2 (Fig. 4D–G). XANES spectra collected at different spots in the sample were all similar and displayed some ionic characteristics (Fig. 4C). Linear combination analyses showed that minor metallic Au was present in addition to C-bound Au (Table 2).

Gold anomalous calcrete samples from the White Dam mineralization were screened using LA–ICP–MS to assess the distribution of Au in calcrete from a site climatically and geologically similar to Barns. In bulk analyses concentrations of Au in calcrete ranged from below detection to several 100 μg kg^{-1}. Based on LA–ICP–MS a 'hotspot' with a Au concentration of several g kg^{-1} was detected, suggesting the presence of particulate Au. μXRF mapping confirmed this result and showed that, similarly to the observations of Lintern et al. (2009), Au occurred in proximity to highly calcareous zones (up to 40 wt.% Ca) but the maxima of Au and Ca did not coincide, and no direct correlation was observed (correlation coefficient of −0.2 between Au and Ca, Fig. 6C–F). Other trace metals, i.e., Zn, Cu and Ni showed no correlation to Au (correlation coefficient of −0.2), which is typical of calcrete samples. XANES spectroscopy confirmed the presence of metallic Au at the hotspots (Fig. 6B). In an area surrounding a Au hotspot ionic Au was observed (Fig. 6B and Table 2).

4. DISCUSSION

4.1. Implications for the formation of Au anomalous Ca carbonates

The ubiquity and abundance of biogenic morphologies in calcrete from the Barns prospect and other Australian and international sites demonstrate that microbial processes are important for the formation of calcrete (e.g.,

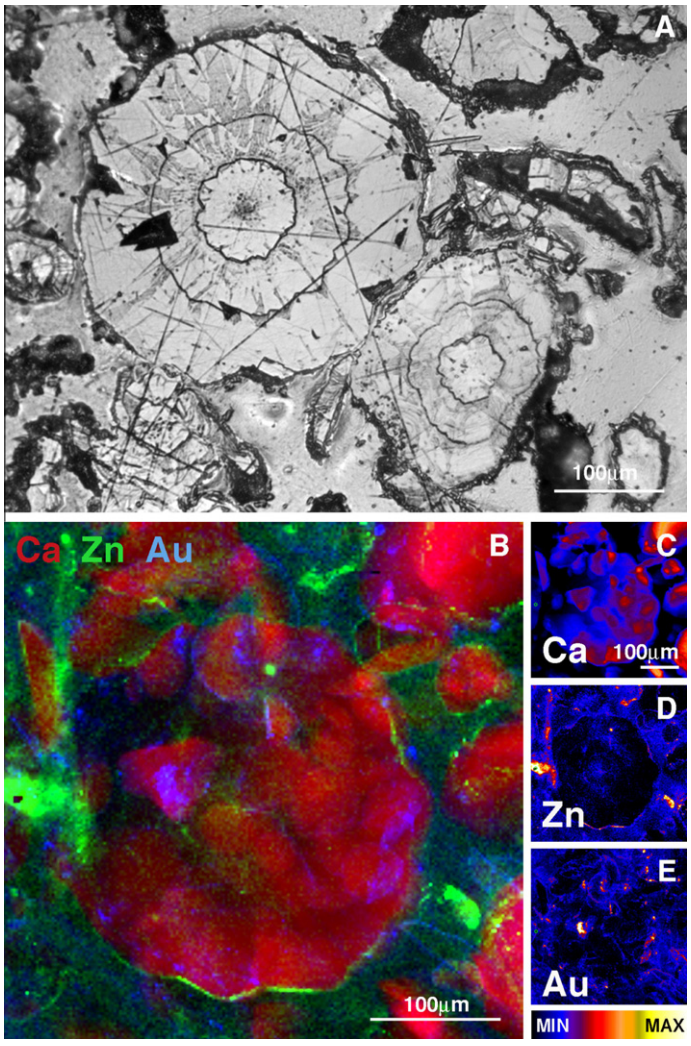

Fig. 2. Spherical zoned biogenic Ca carbonate crystal formed by active bacterial cells in urea medium amended with Au(III)-chloride$_{aq}$ (Experiment 2). Optical micrograph (A), high resolution μXRF maps RGB-overlay, Ca, red; Zn, green, Au blue (C) and individual element maps, Ca (D), Zn (E), Au (F); maximum concentrations for the Ca, Zn and Au are 125.0 ± 1.0 g kg^{-1}, 2.7 ± 0.2 mg kg^{-1} and 8.8 ± 0.1 mg kg^{-1}, respectively. (For interpretation of the references in colour in this figure legend, the reader is referred to the web version of this article.)

Phillips et al., 1987; Zhou and Chafetz, 2009). In Barns samples the most common biogenic morphologies consist of mats of calcified rod-shaped cells coated with μ-crystals of calcite, which closely resembled Ca carbonates precipitated by active bacterial cells in our laboratory experiments. However, studying morphologies alone does not resolve if the formation of these Ca carbonates depends on microbial activity or if their formation is the result of passive processes.

Studying the mineralogy of precipitated Ca carbonates and comparing it to calcrete pointed towards active microbial processes being involved in their formation. Calcite is the main Ca carbonate polymorph detected in experiments with active bacterial cultures as well as in calcrete at Barns and many other Australian sites (Milnes and Hutton, 1983; Schmidt Mumm and Reith, 2007). In contrast, in the presence of dead cells hydroxylapatite was formed. Formation of hydroxylapatite in the presence of organic matter derived from microbial cells has been observed in soils and sediments, and does not require active microbial cells (Hirschler et al., 1990). In the experiments with active cells in the absence of Au complexes approximately 20 wt.% spherical vaterite was formed. Inducing higher pCO_2 in the absence of cells also led to the formation of spherical vaterite, suggesting that vaterite formation was biologically-induced via the release of CO_2. Increasing pH or Ca supersaturation through evaporation in the absence of cells did not lead to the formation of Ca carbonates. These results show that active biochemical processes are required for the formation of calcite in incubation experiments, and suggest that active microbial processes as well as living cells are required for the formation of calcrete, hence expanding conclusions drawn by Reith et al. (2009b). In their previous study Reith et al. (2009b) concluded that microbiota fulfilled two important functions in Ca carbonatogenesis: Firstly microbial activity is required to alter solution chemistry, and

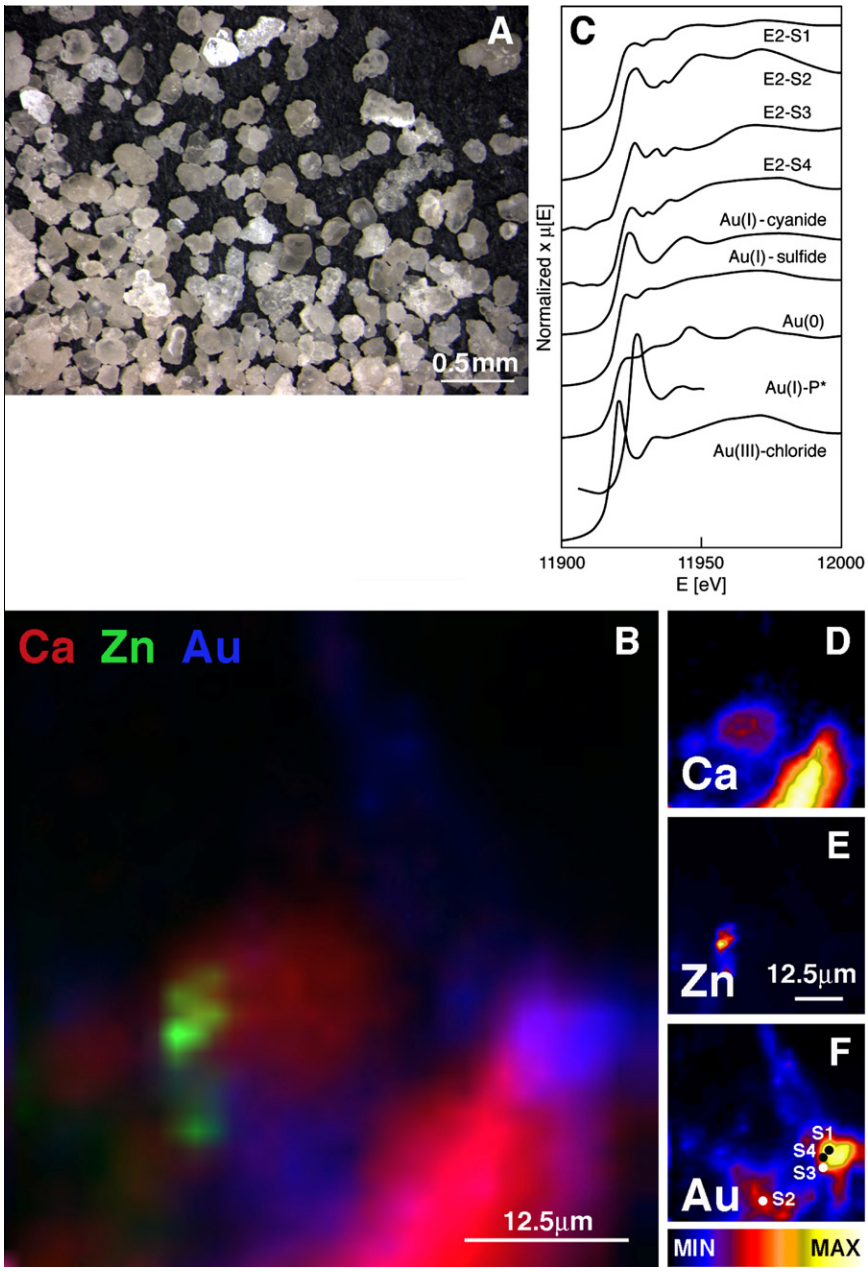

Fig. 3. Ca carbonate crystals formed by active bacterial cells in urea medium amended with Au(III)-chloride$_{aq}$ (Experiment 2). Optical micrograph (A), μXRF maps RGB-overlay, Ca, red; Zn, green; Au, blue (B); XANES spectra of Au (C) and individual element maps, Ca (D), Zn (E), Au (F); maximum concentrations for the Ca, Zn and Au are 81.0 ± 0.2 g kg^{-1}, 405.6 ± 5.0 mg kg^{-1} and 78.9 ± 0.5 mg kg^{-1}, respectively. (For interpretation of the references in colour in this figure legend, the reader is referred to the web version of this article.)

secondly cells were required for nucleation of Ca carbonates, yet it had remained unclear if living or dead cells or cell components would suffice.

Result of this study show that the concentration and distribution of Au in individual Ca carbonates precipitated by active cells is homogenous at the spatial resolution possible with LA–ICP–MS (>30 μm^2), but that is varies considerably between different crystals. This was also observed in samples measured by Reith et al. (2009b). The differences in Au concentrations detected between different crystals from the same experiment suggest a relationship between the concentration of Au and Ca remaining in the solution with the timing and duration of Ca carbonate crystal formation. Synchrotron μXRF mapping and μXANES spectroscopy were undertaken to assess the distribution and speciation Au in Ca carbonates precipitated by active cultures, by raising pCO_2 and in calcrete from White Dam. In addition, the nature of the association between Au, Ca and other metals at μm-scale in experiments amended with Au(III)-chloride and Au-amino acid complexes was

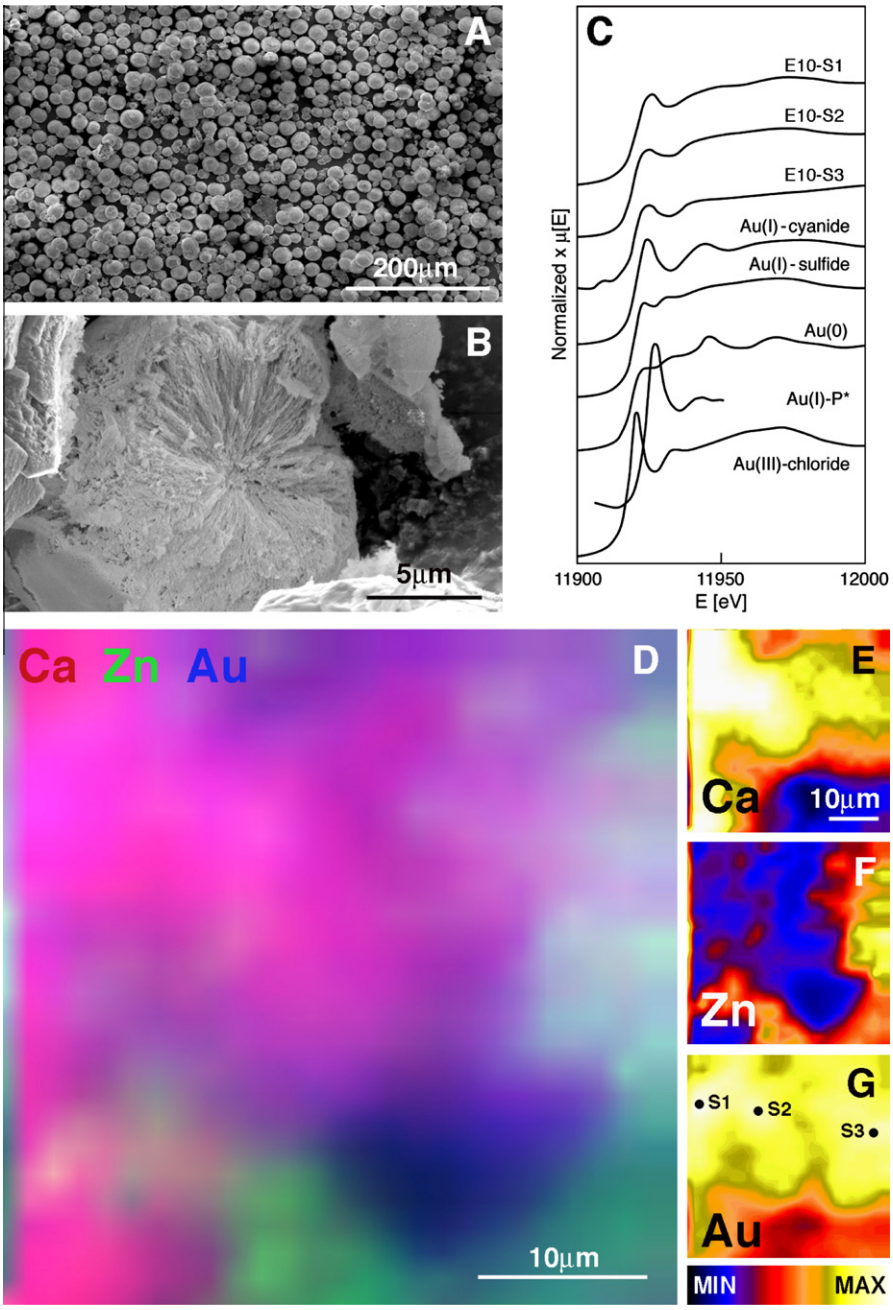

Fig. 4. Spherical vaterite formed in urea medium amended with Au(III)-chloride$_{aq}$ with increased pCO_2 of abiogenic Ca carbonates (Experiments 9 and 10). Secondary electron micrographs (A and B), XANES spectra of Au (C) and µXRF maps RGB-overlay, Ca, red; Zn, green, Au blue (D) and individual element maps, Ca (E), Zn (F), Au (G) of vaterite formed in Experiment 10; maximum concentrations for the Ca, Zn and Au are 93.5 ± 0.6 g kg^{-1}, 187.5 ± 0.3 mg kg^{-1} and 143.1 ± 0.3 mg kg^{-1}, respectively. (For interpretation of the references in colour in this figure legend, the reader is referred to the web version of this article.)

evaluated. To be able to compare our data to the results published by Lintern et al. (2009), µXRF-maps and XANES spectra were collected at the same beamline using similar procedures. At sub-µm resolution the distribution of Au in calcite formed by active cultures was not uniform and numerous 'Au hotspots' were observed independent of the Au-complex used, mimicking the distribution of Au in calcrete from White Dam (this study) and Bounty deposit in Western Australia (Lintern et al., 2009). Spatial correlation of Au- with Ca- and Zn concentrations observed in calcite precipitated by active cultures were weak, reflecting similar findings in natural samples (this study, Lintern et al., 2009). In contrast, in abiogenically formed Ca carbonates a strong µm-scale correlation of Au and Ca was observed. These results further demonstrate that bacterial activity is required for the formation of Au-anomalous Ca-carbonates, in

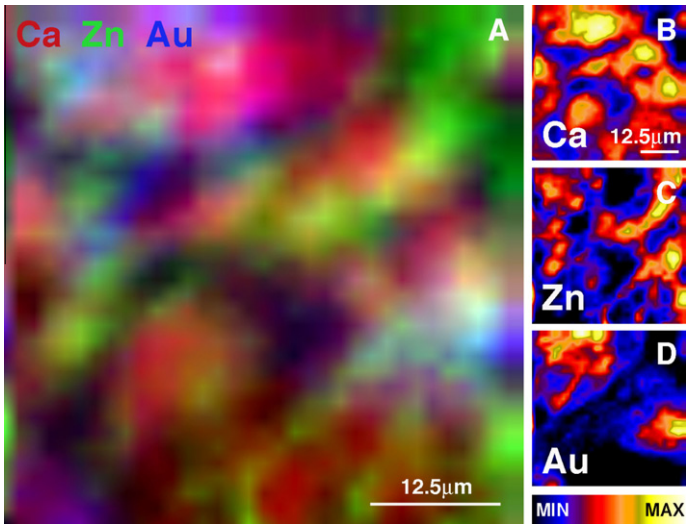

Fig. 5. (A) µXRF maps of Au in biogenic Ca carbonates formed in urea growth media with amended with Au-aspartic acid complexes (Experiment 3), RGB-overlay, Ca, red; Zn, green, Au blue) and individual element maps, Ca (B), Zn (C), Au (D); maximum concentrations for the Ca, Zn and Au are 208.5 ± 1.0 g kg^{-1}, 18.0 ± 0.1 mg kg^{-1} and 4.8 ± 0.1 mg kg^{-1}, respectively. (For interpretation of the references in colour in this figure legend, the reader is referred to the web version of this article.)

which the Au distribution mimics that of natural calcrete. Because decoupling of Au and Ca was also observed in Ca carbonates from experiments amended with Au(III)-chloride complexes, our results suggest that the geomicrobial model for Au-anomalous Ca carbonate precipitation, which currently includes Au-amino-acid complexes (Reith et al., 2009b), should be extended to cover a range of environmentally important Au(I/III)-halide complexes.

The shape of the XANES spectra as well as the location of the different Au species observed in calcite precipitated by active cells closely resembled those observed in calcrete (this study; Lintern et al., 2009). This was confirmed with LCF, which showed both C-bound and metallic Au. XANES spectra of ionic Au in calcrete and in Ca carbonates precipitated by active cells also resembled spectra obtained from *C. metallidurans* cells after 120 h of incubation (Reith et al., 2009a; Table 2). Reith et al. (2009a) showed that Au detoxification in bacterial cells occurred via a combination of efflux, reduction, and possibly methylation of Au(III)-complexes, leading to the formation of Au(I)-C-compounds and metallic Au(0). This suggests that reductive precipitation of Au by bacterial cells combined with Ca carbonatogenesis may be involved in the formation of Au-anomalous Ca carbonates.

4.2. Assessment of current models for the formation of Au anomalous calcrete

In order to form Au-anomalous calcrete in its pedogenic setting, Au and Ca have to be mobilized, transported and precipitated and Ca carbonate has to be formed. There is good agreement about the sources of Ca, carbonate and Au: field- and experimental studies have shown Ca from marine sources and weathering bedrock; and carbonate from C3- and C4 plants, and that Au is sourced from underlying mineralization; (e.g., Lintern et al., 2006; Dart et al., 2007). In arid, surficial environments, down to 500 m below the land surface, chemolithoautotrophic iron- and sulfur-oxidizing bacteria, such as *A. ferrooxidans* and *A. thiooxidans*, and archaea, form biofilms on metal sulfides (Enders et al., 2006). These biofilms mediate the formation thiosulfate, which in the presence of oxygen can lead to oxidation, complexation and mobilization of Au (Aylmore and Muir, 2001; Reith et al., 2007). These mobile Au complexes may then be transported with fluctuating groundwater until they reach plant roots, where they are taken up. Hence, evapotranspiration is likely to play an important role for Au transport from the underlying mineralization to the place of Ca carbonatogenesis (Lintern et al., 2006, 2009). However, Lintern et al. (2006, 2009) extended the evapotranspiration-based model to also explain the precipitation of Ca carbonates as well as the associated distribution and speciation of Au. While evapotranspiration is clearly important for the transport of Au, it does not explain the actual precipitation of Au-anomalous calcrete with its Au–Ca association; an association that is not apparent in other evaporation-driven environments. In contrast, the geomicrobial model proposed by Schmidt Mumm and Reith (2007) and experimentally verified by Reith et al. (2009b) is capable of explaining these mechanisms. The new experimental results presented here show that only the metal distribution and speciation in biologically produced Au-bearing carbonates are consistent with observations made in this study and by Lintern et al. (2009) regarding (i) the location of the Ca carbonate formation and association of (ii) Au in calcrete:

(i) High concentrations of Au ('hotspots') were associated with a calcified root tubule (rhizomorph) in a calcrete sample from the Bounty deposit in Western Australia, and were interpreted by Lintern et al. (2009) to result from deposition in high porosity channels through inorganic processes upon evaporation. However, rhizomorphs form through the interaction of microbial communities with environmental

Table 2
Results of linear combination analyses (LCF) of XANES Au spectra from Ca carbonates precipitated by active cell, after raising pCO_2 as well as natural calcrete samples. Au model substances in are metallic Au(0), Au(I)-sulfide, Au(I)-P ($[Au(PPh_2Me)_4]^+$; Elder and Eldsness, 1987), Au(I)-cyanide, Au(III)-chloride/-hydroxide; given are mole fractions ± standard deviation.

Experiment/location	Spectrum	Au(0)	Au(I)-sulfide	Au(I)-cyanide	Au(I)-P[e]	Au(III)-chloride/hydroxide	R-factor	Chi^2
E2[a]	S1	0.17 ± 0.14	0	0.83 ± 0.14		0	0.06	1.45
	S2	0.18 ± 0.01	0	0.69 ± 0.01	0.15 ± 0.01	0	0.03	0.93
	S3	0.62 ± 0.09	0	0	0.31 ± 0.04	0	0.01	0.51
	S4	0.92 ± 0.01	0	0	0.08 ± 0.01	0	0.002	0.06
E10[b]	S1	0.56 ± 0.02	0	0.44 ± 0.02	0	0	0.001	0.04
	S2	0.35 ± 0.04	0	0.65 ± 0.04	0	0	0.004	0.16
	S3	0.31 ± 0.01	0	0.69 ± 0.01	0	0	0.01	0.28
White Dam[c]	S1	0.82 ± 0.04	0	0.16 ± 0.04	0	0	0.003	0.10
	S2	0.91 ± 0.01	0	0	0.09 ± 0.01	0	0.0007	0.03
	S3	0.55 ± 0.13	0	0.45 ± 0.13	0	0	0.05	1.20
Bounty[d]	Halo 1	0.61 ± 0.07	0	0.17 ± 0.06	0.22 ± 0.03	0	0.003	0.06
	Halo 2	0.26 ± 0.08	0.31 ± 0.07	0.37 ± 0.03	0	0	0.0008	0.02
	Halo 3	0.56 ± 0.04	0	0.23 ± 0.04	0.22 ± 0.02	0	0.001	0.02

[a] Spectra and locations shown in Fig. 3C.
[b] Spectra and locations shown in Fig. 4C.
[c] Spectra and locations shown in Fig. 6C.
[d] Spectra obtained after digitalization of Fig. 15 (Lintern et al., 2009).
[e] Digitalized from Elder and Eldsness (1987).

solutions and plants in the rhizosphere, which is the zone of highest microbal activity in soils (Phillips et al., 1987; Manning, 2008). These rhizosphere communities are highly enriched with respect to heterotrophic microbiota and are sustained by the decomposition of plant tissue and plant root exudation (Berg and Smalla, 2009). Plants exude high concentrations of low molecular weight organic acids, amino acids, amino sugars, proteins and other short chained organic molecules through their roots into the surrounding rhizosphere (Jones, 1998). These may directly or indirectly lead to the mobilization of major and trace metals, which in their ionic forms are taken up as nutrients by the plant roots (Khan, 2005). However, microbial rhizosphere communities are known to rapidly utilize these compounds, and because of this activity also control metal mobilization and precipitation as well as the biomineralization of new minerals, e.g., Ca carbonates (Jones, 1998; Wenzel et al., 2004). One of the pathways most commonly utilized by heterotrophic communities is the ureolysis pathway which leads to Ca carbonatogenesis by inducing geochemical conditions favorable for the formation of Ca carbonates on cell surfaces, which act as nucleation sites (Castanier et al., 1999, 2000). This is supported by C-isotope ratios in auriferous calcrete from a site located in close proximity to Barns, which showed that C in calcrete was isotopically light and originated from organic compounds initially formed by C3 and C4 plants (Lintern et al., 2006). These compounds were subsequently mineralized to inorganic C by heterotrophic processes and re-precipitated in the vicinity of the roots as rhizomorphs or other biogenic carbonates by rhizosphere communities. Naturally, the Au-complexes-amino-acid-urea decomposition model is not the only pathway that can lead to the formation of Au-anomalous calcrete, rather it is one of several microbial pathways leading to the formation of Ca carbonates that occur successively or simultaneously in the surface- and rhizosphere soils (Castanier et al., 1999).

(ii) Lintern et al. (2009) observed a correlation between ionic Au and Br in rhizomorphic calcrete from the Bounty deposit and suggested a mechanistic link. This, they claim, validates the evapotranspirative model for Au-anomalous calcrete formation. Indeed, ionic Au may occur as Au(I/III)-hydroxo-chloro-bromide-complexes in oxidizing groundwaters with high halide concentrations, i.e., Cl^- and Br^-, which are typically found in semi-arid and arid zones (Krauskopf, 1951; Usher et al., 2009). However, the present study also shows a direct link between Ca carbonate formation by active cells and Au(III)-halide precipitation. Experiment 2, which was amended with a Au(III)-chloride complex showed that the active bacterial cultures were capable of precipitating Au-anomalous Ca carbonates, which displayed a similar distribution and speciation Au as that observed in calcrete from White Dam (this study) and the Bounty deposit (Lintern et al., 2009). Organic matter and microbiota have a much higher affinity for mobile Au complexes than mineral phases (Reith and McPhail, 2006, 2007; Reith et al., 2007). This suggests that the precipitation of mobile Au-complexes in the presence of large numbers of microbiota that are present in the root zone is the result of microbial processes. This argument is supported by linear combination analyses of the ionic Au spectra published by Lintern et al. (2009), which show that the ionic Au in their study is not present as Au(I/III)-hydroxo-chloro-bromide-complexes, as would be expected based if a direct mechanistic link existed. In contrast, Au in calcrete was present as a combination of C-, P- and S-bound- and metallic Au,

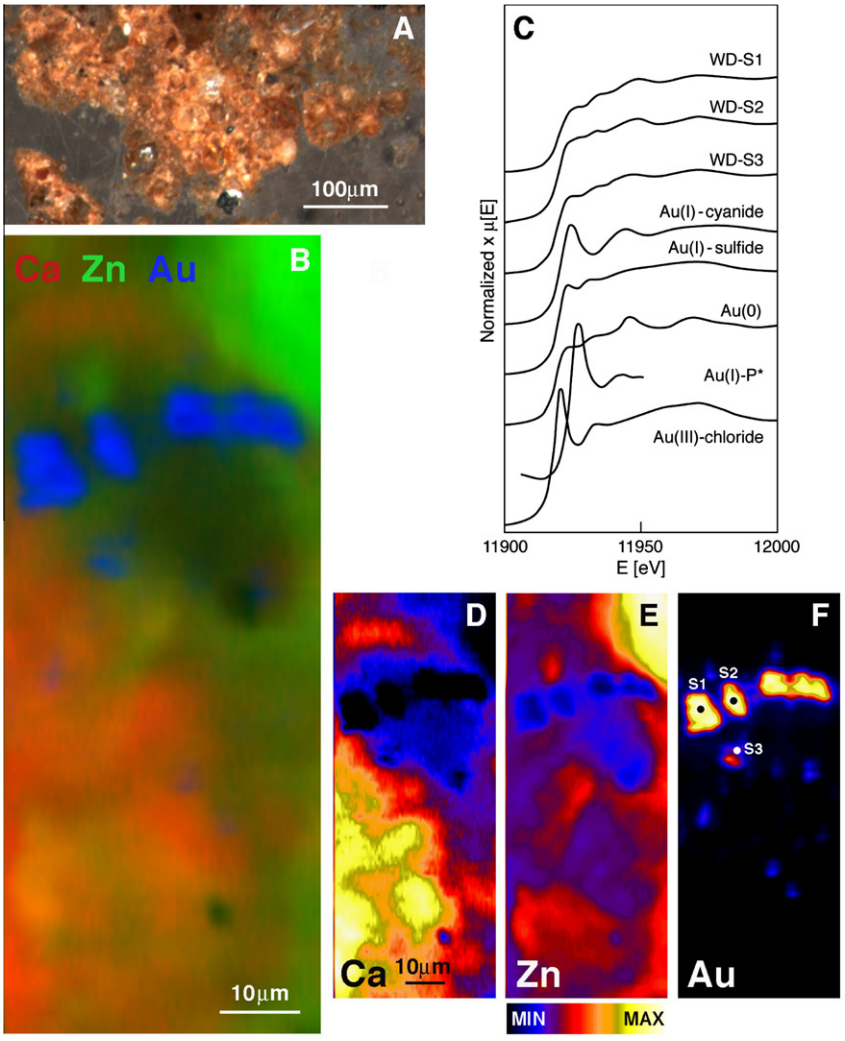

Fig. 6. Optical micrograph of natural calcrete from White Dam, South Australia Ca-carbonates (A), µXRF maps RGB-overlay, Ca, red; Zn, green, Au blue) (B); XANES spectra of Au (C) and individual element maps Ca (D), Zn (E), Au (F); maximum concentrations for the Ca, Zn and Au are 50.5 ± 0.2 g kg^{-1}, 261.6 ± 0.2 mg kg^{-1} and 2.0 ± 0.1 g kg^{-1}, respectively. (For interpretation of the references in colour in this figure legend, the reader is referred to the web version of this article.)

similar to Au in Ca carbonates precipitated by active enrichment cultures and *C. metallidurans* (Reith et al., 2009a). Many bacteria and archaea are capable of passively adsorbing or actively catalyzing the reductive precipitation of Au(I/III)-complexes as shown in numerous studies (Reith et al., 2009a; Southam et al., 2009 and references therein). While passive sorption to bacterial and fungal cells is a mechanism that may lead to the observed Au distribution, the differences in Au speciation observed from hotspot (metallic Au) to its halo increasing proportions of ionic Au in biogenic carbonates and calcrete may suggest that active reductive precipitation of Au(III)-complexes to metallic Au via intermediate Au(I)- complexes occurred, similar to a study by Reith et al. (2009a). This cell-driven adsorption of Au-complexes is likely to occur simultaneously to formation of calcite crystals on cells, to which subsequent to their entombment further Au is sorbed, which is not further reduced, hence forming observed metallic hotspots and ionic haloes. Another explanation for the formation of metallic hotspots with haloes of ionic Au may lie in weathering of primary metallic Au, which had been physically transported to the weathering site. In the presence of active bacterial Au mobilization and complexation to amino-acids, cyanide and S-components or formation of nano-particles may occur, which may lead to a similar Au speciation (Reith and McPhail, 2006, 2007; Lintern et al., 2009; Reith et al., 2010). However, at the Barns site this is unlikely, as Lintern et al. (2009) clearly documented an autochthonous pathway in which Au has been chemically transported.

5. CONCLUSIONS

Biogenic Ca carbonates are ubiquitous and highly abundant in calcrete from Barns and other Australian sites,

which is consistent with earlier observations that biological processes drive the formation of calcrete in these environments. The results presented in this paper demonstrate that active bacteria produce Ca carbonates that display a mineralogy, Au-, Ca- and base metal distribution and Au speciation similar to that observed in calcrete. In contrast, experiments conducted without active cells failed to reproduce these features. In conclusion, these results show that microbial processes are driving forces behind the actual biomineralization of Au anomalous calcrete and are not, as previously suggested, incidental to its formation.

ACKNOWLEDGMENTS

The authors acknowledge the following individuals and institutions for their contributions: Advanced Photon Source (APS), and the Australian Synchrotron (AS) for provision of beamtime, the Australian Research Council (ARC) and the Australian Synchrotron Research Funding Schemes for funding this project; CSIRO Land and Water for the use of the microbial ecology laboratory; L. Green and A. Netting at Adelaide Microscopy for their assistance with the (FIB)–SEM and LA–ICP–MS. Use of the APS was supported by the US Department of Energy, Office of Science, Office of Basic Energy Sciences, under Contract No. DE-AC02-06CH11357. This forms TRaX Record 138.

REFERENCES

Achyuthan H. (2003) Petrologic analysis and geochemistry of the Late Neogene-Early Quaternary hardpan calcretes of Western Rajasthan, India. *Quart. Internat.* **106**, 3–10.

Australian Government, Bureau of Meteorology, 2005. Climate Averages for Australian Sites – Averages for South Australian Sites, 018044KYANCUTTA, <http://www.bom.gov.au/climate/averages/tables/ca_sa_names.shtml>.

Australian Government, Bureau of Meteorology, 2010. Climate Averages for Australian Sites – Averages for South Australian Sites. <http://www.bom.gov.au/climate/averages/tables/cw_020026.shtml>.

Aylmore M. G. and Muir D. M. (2001) Thiosulfate leaching of gold – a review. *Miner. Eng.* **14**, 135–174.

Berg G. and Smalla K. (2009) Plant species and soil type cooperatively shape the structure and function of microbial communities in the rhizosphere. *FEMS Microbiol. Ecol.* **68**, 1–13.

Boquet E., Boronat A. and Ramos-Cormenzana A. (1973) Production of calcite (calcium carbonate) crystals by soil bacteria is a general phenomenon. *Nature* **246**, 527–529.

Braissant O., Cailleau G., Dupraz C. and Verrecchia A. P. J. (2003) Bacterially induced mineralization of calcium carbonate in terrestrial environments: The role of exopolysaccharides and amino acids. *J. Sedimentary Res.* **73**, 485–490.

Butt C. R. M. and Smith R. E. (1992) Characteristics of the weathering profile – Exploration in Calcrete Terrain. In Handbook of Exploration Geochemistry. Regolith Exploration Geochemistry in Tropical and Subtropical Terrains (eds. C. R. M. Butt and H. Zeegers). Amsterdam, London. 608 pp.

Castanier S., Le Me'tayer-Levrel G. and Perthuisot J. P. (1999) Ca-carbonates precipitation and limestone genesis – the microbiogeologist point of view. *Sedimen. Geol.* **126**, 9–23.

Castanier S., Le Me'tayer-Levrel G. and Perthuisot J.-P. (2000) Bacterial roles in the precipitation of carbonate minerals. In *Microbial Sediments* (eds. R. E. Riding and S. M. Awramik). Springer-Verlag, Heidelberg, Germany, pp. 32–39.

Cooke A. (2003) White Dam – an exciting new gold project in the Curnamona Province. *MESA J.* **31**, 46–47.

Dart R. C. (2009) Gold-in-calcrete: A continental to profile scale study of regolith carbonates and their association with gold mineralisation. Ph.D. thesis, University of Adelaide.

Dart R. C., Barovich K. M., Chittleborough D. J. and Hill S. M. (2007) Calcium in regolith carbonates of central and southern Australia: Its source and implications for the global carbon cycle. *Palaeogeograph. Palaeoclim. Palaeoecol.* **249**, 322–334.

Drown C. G. (2003) The Barns Gold Project – discovery in an emerging district. Quarterly Earth Resources Journal of Primary Industries and Resources South Australia. *MESA J.* **28**, 4–9.

Elder R. C. and Eldsness M. K. (1987) Synchrotron X-ray studies of metal-based drugs and metabolites. *Chem. Rev.* **87**, 1027–1046.

Enders M. S., Southam G., Knickerbocker C. and Titley S. R. (2006) The role of microorganisms in the supergene environment of the Morenci porphyry copper deposit, Greenlee County, Arizona. *Econ. Geol.* **101**, 59–70.

Flint D. J. and Parker A. J. (1993) Willyama Inliers. In *The geology of South Australia; vol. 1, The Precambrian* (eds. J. F. Drexel, W. V. Preiss and A. J. Parker). Geolog. Surv. South Australia, Adelaide, pp. 82–93.

Hammes F., Boon N., de Villiers J., Verstratet W. and Siciliano S. D. (2003) Strain-specific ureolytic microbial calcium carbonate precipitation. *Appl. Environ. Microbiol.* **69**, 4901–4909.

Hill S. M., McQueen K. G. and Foster K. A. (1998) Regolith carbonate accumulations in western and central NSW: characteristics and potential as an exploration sampling medium. In *Regolith 98, Australian Regolith & Mineral Exploration: New Approaches to an Old Continent* (eds. G. M. Taylor and C. F. Pain). WMC Conference centre, Kalgoorlie, Western Australia, pp. 191–206 .

Hirschler A., Lucas J. and Hubert J. C. (1990) Bacterial involvement in apatite genesis. *FEMS Microbiol. L* **73**, 211–220.

Khan A. G. (2005) Role of soil microbes in the rhizosphere of plants growing on trace metal contaminated soils in phytoremediation. *J. Trace Elem. Med. Biol.* **18**, 355–364.

Königsberger E., Königsberger L. C. and Gamsjäger H. (1999) Low-temperature thermodynamic model for the system Na_2CO_3–$MgCO_3$–$CaCO_3$–H_2O. *Geochim. Cosmochim. Acta* **63**, 3105–3119.

Krauskopf K. B. (1951) The solubility of gold. *Econ. Geol.* **46**, 858–870.

Krumbein W. E. (1979) Calcification by bacteria and algae. In *Biogeochemical Cycling of Mineral-Forming Elements* (eds. P. A. Trudinger and D. J. Swaine). Elsevier, Amsterdam, pp. 47–68.

Jones D. L. (1998) Organic acids in the rhizosphere – a critical review. *Plant and Soil* **205**, 25–44.

Langmuir D. (1997) *Aqueous Environmental Geochemistry*. Prentice Hall, Upper Saddle River, NJ, 600 pp..

Lengke M. F., Ravel B., Fleet M. E., Wanger G., Gordon R. A. and Southam G. (2006) Mechanisms of gold bioaccumulation by filamentous cyanobacteria from gold(III)-chloride complex. *Environ. Sci. Technol.* **40**, 6304–6309.

Lintern M. J. (2001) Exploration for gold using calcrete – lessons from the Yilgarn Craton, Western Australia. *Geochem. Explor. Environ. Anal.* **1**, 237–252.

Lintern M. J. and Butt C. R. M. (1993) Pedogenic carbonate: An important sampling medium for gold exploration in semi-arid areas. *Explor. Res. News* **7**, 7–11.

Lintern M. J., Hough R. M., Ryan C. G., Watling J. and Verrall M. (2009) Ionic gold in calcrete revealed by LA–ICP–MS, SXRF and XANES. *Geochim. Cosmochim. Acta* **73**, 1666–1683.

Lintern M. J., Sheard M. J. and Chivas A. R. (2006) The source of pedogenic carbonate associated with gold-calcrete anomalies in the western Gawler Craton, South Australia. *Chem. Geol.* **235**, 299–324.

Manning D. A. C. (2008) Biological enhancement of soil carbonate precipitation: Passive removal of atmospheric CO_2. *Miner. Mag.* **72**, 639–649.

Martín-Algarra A. and Sánchez-Navas A. (2000) Bacterially mediated authigenesis in Mesozoic stromatolites from condensed pelagic sediments (Betic Cordillera, Southern Spain). In Marine Authigenesis: From Global to Microbial (eds. C. R. Glenn, J. Lucas and L. Prévot-Lucas). S.E.P.M. Special Publication 66. pp. 499–525.

McQueen K. G., Hill S. M. and Foster K. A. (1999) The nature and distribution of regolith carbonate accumulations in southeastern Australia and their potential as a sampling medium in geochemical exploration. *J. Geochem. Explor.* **67**, 67–82.

Milnes A. R. and Hutton J. T. (1983) Calretes in Australia. In Soils: An Australian Viewpoint, CSIRO. Academic Press, London, New York. pp. 119–162.

Morita R. Y. (1980) Calcite precipitation by marine bacteria. *Geomicrobiol. J.* **2**, 63–82.

Moussavi-Harami R., Mahboubi A., Nadjafi M., Brenner R. L. and Mortazavi M. (2009) Mechanism of calcrete formation in the Lower Cretaceous (Neocomian) fluvial deposits, northeastern Iran based on petrographic, geochemical data. *Creteac. Res.* **30**, 1146–1156.

Phillips S. E., Milnes A. R. and Foster R. C. (1987) Calcified Filaments: An example of biological influences in the formation of calcrete in South Australia. *Aust. J. Soil Res.* **25**, 405–428.

Ravel B. and Newville M. (2005) Athena, Artemis, Hephaestus: Data analysis for X-ray absorption spectroscopy using Ifeffit. *J. Synchr. Radiat.* **12**, 537–541.

Reith F., Etschmann B., Grosse C., Moors H., Benotmane M. A., Monsieurs P., Grass G., Doonan C., Vogt S., Lai B., Martinez-Criado G., George G. N., Nies D., Mergeay M., Pring A., Southam G. and Brugger J. (2009a) Mechanisms of gold biomineralization in the bacterium Cupriavidus metallidurans. *Proc. Natl. Acad. Sci.* **106**, 17757–17762.

Reith F., Fairbrother L., Nolze G., Wilhelmi O., Clode P., Gregg A. L., Parsons J. E., Wakelin S. A., Pring A., Hough R., Southam G. and Brugger J. (2010) Nanoparticle factories: Biofilms hold the key to gold dispersion and nugget formation. *Geology* **38**, 843–846.

Reith F., Lengke M. F., Falconer D., Craw D. and Southam G. (2007) Winogradski review – the geomicrobiology of gold. *ISME J.* **1**, 567–584.

Reith F. and McPhail D. C. (2006) Effect of resident microbiota on the solubilization of gold in soil from the Tomakin Park Gold Mine, New South Wales, Australia. *Geochim. Cosmochim. Acta* **70**, 1421–1438.

Reith F. and McPhail D. C. (2007) Microbial influences on solubilisation and mobility of gold and arsenic in regolith samples from two gold mines in semi-arid and tropical Australia. *Geochim. Cosmochim. Acta* **71**, 1183–1196.

Reith F., Wakelin S., Gregg A. L. and Schmidt Mumm A. (2009b) A microbial pathway for the formation of gold anomalous calcrete. *Chem. Geol.* **258**, 315–326.

Rivadeneyra M. A., Delgado R., Delgado G., Del Moral A., Ferrer M. R. and Ramos-Cormenzana A. (1993) Precipitation of carbonate by *Bacillus* sp. isolated from saline soils. *Geomicrobiol J.* **11**, 175–184.

Ryan C. G. (2000) Quantitative trace element imaging using PIXE and the nuclear microprobe. *Int. J. Imag. Syst. Technol.* **11**, 219–230.

Ryan C. G. and Jamieson D. N. (1993) Dynamic analysis: On-line quantitative PIXE microanalysis and its use in overlap-resolved elemental mapping. *Nucl. Instrum. Methods Phys. Res. Sec. B* **B77**, 203–214.

Ryan C. G., Etschmann B. E., Vogt S., Maser J., Harland C. L., Van Achterbergh E. and Legnini D. (2005) Nuclear microprobe-synchrotron synergy: Towards integrated quantitative real-time elemental imaging using PIXE and SXRF. *Nucl. Instrum. Methods Phys. Res. Sec. B* **B231**, 183–188.

Schmidt Mumm A. and Reith F. (2007) Calcrete genesis at the gold anomaly of the Barns prospect, Gawler Craton, South Australia. *J. Geochem. Explor.* **92**, 13–33.

Southam G., Lengke M. F., Fairbrother L. and Reith F. (2009) The biogeochemistry of gold. *Elements* **5**, 303–307.

Stumm W. and Morgan J. J. (1996) Aquatic Chemistry. Chemical equilibria and rates in natural waters, 3rd ed., Wiley.

Twidale C. R. and Wopfner H. (1990) Dunefields. In *Natural History of the North East Deserts* (eds. M. J. Tyler, C. R. Twidale, M. Davies and C. B. Wells). Royal Soc. Australia, Adelaide, pp. 45–60.

Usher A., McPhail D. C. and Brugger J. (2009) A spectrophotometric study of aqueous Au(III) halide-hydroxide complexes at 25–80 °C. *Geochim. Cosmochim. Acta* **73**, 3359–3380.

Wenzel W. W., Lombi E. and Adriano D. C. (2004) Biogeochemical processes in the rhizosphere: Role in phytoremediation of metal-polluted soils. In *Heavy Metal Stress in Plants: From Biomolecules to Ecosystems* (eds. M. Prasad and J. Hagemeyer). Springer Verlag, Berlin, Heidelberg, New York, pp. 273–303.

Wright V. P. (1997) A micromorphological classification of fossil and recent calcic and petrocalcic microstructures. In *Soil Micromorphology: A Basic and Applied Science: Developments in Soil Science*, vol. 19 (ed. L. A. Douglas). Elsevier, Amsterdam, pp. 401–407.

Zavarin G. A. (2000) Microbial geochemical calcium cycle. *Microbiology* **71**, 5–22.

Zhou J. and Chafetz H. S. (2009) Biogenic caliches in Texas: The role of organisms and effect of climate. *Sediment. Geol.* **222**, 207–225.

Associate editor: Johnson R. Haas